A Letters Journal Exploring the Frontiers of Physics

December 2018

EPL, **124** (2018) 56001
doi: 10.1209/0295-5075/124/56001

www.epljournal.org

Cation distribution of Mn-Zn ferrite nanoparticles using pair distribution function analysis and resonant X-ray scattering

Rodrigo U. Ichikawa[1(a)], João P. R. L. L. Parra[2], Oriol Vallcorba[3], Inma Peral[4,5], Walter K. Yoshito[1], Margarida J. Saeki[2], Xavier Turrillas[3,6] and Luis G. Martinez[2]

[1] *Nuclear and Energy Research Institute, Materials Science and Technology Center(IPEN-CNEN) Av Lineu Prestes 2242, 05508-000 São Paulo-SP, Brazil*
[2] *São Paulo State University, Institute of Biosciences(UNESP-IBB) - Via Domingos Sartor, Km 4, 18618-970, Botucatu-SP, Brazil*
[3] *ALBA Synchrotron - Carrer de la Llum, 2-26, 08290 Cerdanyola del Vallès, Barcelona, Spain*
[4] *Université du Luxembourg, Faculté des Sciences, de la Technologie et de la Communication 6 Rue Richard Coudenhove-Kalergi, 1359 Luxembourg, Luxembourg*
[5] *Luxembourg Institute of Science and Technology - 5 Avenue des Hauts-Fourneaux, 4362 Esch-sur-Alzette, Luxembourg, Luxembourg*
[6] *Institut de Ciència de Materials de Barcelona, Department of Crystallography (ICMAB-CSIC) Campus de la UAB 08193 Bellaterra, Spain, 08193 Bellaterra, Barcelona, Spain*

received 15 August 2018; accepted in final form 22 November 2018
published online 27 December 2018

PACS 61.05.cp – X-ray diffraction
PACS 61.46.Hk – Nanocrystals
PACS 61.43.Bn – Structural modeling: serial-addition models, computer simulation

Abstract – Mn-Zn ferrite nanoparticles were synthesized by chemical co-precipitation method and analysed using X-ray synchrotron diffraction data. Pair distribution function (PDF) analysis was used to probe the local structure and revealed that the first-neighbour distances of Fe-Fe and Mn-Zn in the 3.0 up to 3.5 Å range are different from the ones usually reported in the literature. For the sample with the best magnetic behaviour, resonant X-ray scattering (RXS) using three energies close to the absorption edges of Mn, Zn and Fe was applied to determine the cation distribution which explained the previous result from PDF analysis.

Introduction. – Among the numerous applications of $Mn_{1-x}Zn_xFe_2O_4$ nanoparticles we can highlight biomedical applications as magnetic tracer in alternate current biosusceptometry (ACB), magnetic resonance imaging (MRI), for diagnosis of cancer and other diseases as diabetes and Parkinson, whose severity can be monitored by analysing the disturbances of the gastrointestinal motility [1,2]. Specifically, the ACB method is promising because of its low cost, it is non-invasive and because it can be conducted without ionizing radiation. Also, major advances have been achieved by developing a bionanocomposite based on ferrites for the theranostics [3] as well. Recently, we reported that Mn-Zn ferrite nanoparticles with different surface charge can be produced by precipitating them with different NaOH concentrations [2].

In this work, the local structure of five samples precipitated with different NaOH concentrations were analysed using synchrotron X-ray diffraction data. First, pair distribution function (PDF) analysis was applied and the one with best magnetic behaviour was analysed by resonant X-ray scattering (RXS). PDF shows clearly a slight deviation for the peaks representing the first neighbours of Fe-Fe and Mn-Zn (around 3 and 3.5 Å). This can be explained by the sites occupations determined by Rietveld refinement of resonant X-ray scattering data (RXS). It was found that Mn, Zn and Fe are placed at the tetrahedral site (8*a*), while Mn and Fe occupies only the octahedral site (16*d*) of the spinel structure.

Materials and methods. –

Synthesis. Mn-Zn ferrite nanoparticles with nominal composition of $Mn_{0.75}Zn_{0.25}Fe_{2.8}O_4$ were synthesized by

(a) E-mail: ichikawa@usp.br

the chemical co-precipitation method. All reagents used were commercial products with analytical grade (Sigma-Aldrich) manganese (II) nitrate hydrate [$Mn(NO_3)_2 \cdot xH_2O$], zinc nitrate hexahydrate [$Zn(NO_3)_2 \cdot 6H_2O$] and iron chloride hexahydrate($FeCl_3 \cdot 6H_2O$) in deionized water (18.2 MΩcm). The precursor solutions were prepared according to the purposed stoichiometry and dripped in 150 mL of distilled water. The aqueous solutions used as precipitant agent with five different NaOH concentrations (0.05, 0.1, 0.2, 0.5 and 1.00 mol/L) were heated until they boiled. After reaching the desired temperature, the precursor solutions were slowly added into the precipitating solution with stirring for 1 h. The final *p*H in all five cases was controlled assuring that a quantitative precipitation took place, so the NaOH is a variable not interfering with the stoichiometry of the precipitate. The obtained suspensions were separated under magnetic field and centrifuged at 6000 rpm for several times with deionized water and finally with ethanol, to further became as-synthesized powders. The final product was dried and kept in a furnace at 100 °C. The samples were termed MZF005, MZF010, MZF020, MZF050 and MZF100 according to the concentration of NaOH used: 0.05, 0.10, 0.20, 0.50 and 1.00 mol/L, respectively.

Pair distribution function analysis (PDF). With PDF analysis Bragg and diffuse scattering can be treated on an equal basis. Corrections are performed to remove from the powder diffraction measurement extrinsic contributions arising from fluorescence, inelastic and sample holder scattering, etc. Basically, the PDF provides the probability of finding pairs of atoms by a distance r. This probability, termed as $G(r)$, can be obtained by the Fourier transform of the total scattering data, after the pertinent corrections. The relationship between $G(r)$ and the atom pair distance can be given by [4,5]

$$G(r) = \frac{2}{\pi} \int_0^{+\infty} Q[S(Q) - 1] \sin(Qr) \mathrm{d}Q, \qquad (1)$$

where $Q = \frac{4\pi \sin\theta}{\lambda}$ is the scattering vector and $S(Q)$ is the normalized scattering intensity. Then, $G(r)$ can be fitted by models in real space providing insights about the local structure.

Resonant X-ray scattering (RXS). The RXS technique permits the extraction of information about a specific element present in the analysed sample using the variation of its form factor [6,7],

$$f(Q, E) = f_0(Q) + f'(Q, E) + if''(Q, E) \qquad (2)$$

f_0 is the form factor of a free, unperturbed energy-independent atom, f' and f'' are the real and imaginary parts of the resonant term, which correct for the effects of dispersion near the absorption edges, commonly referred to as resonant scattering factors [6]. The terms f' and f'' are usually small when the incident photons have energy far from the absorption edge of the element, however they become very important when the energy is close to the edges and its contribution provides the contrast to obtain specific information about the element occupation. For instance, Rietveld analysis can be applied to refine its atomic positions and occupations more accurately providing information about the atom distribution in the unit cell.

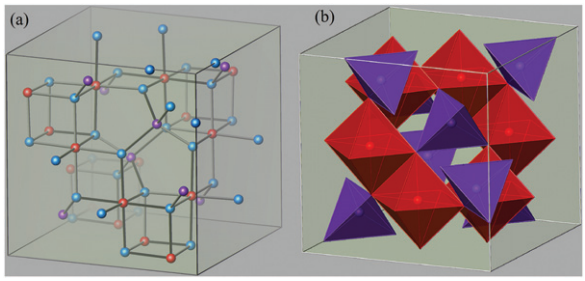

Fig. 1: (Colour online) Spinel crystal structure. Atoms placed in the octahedral site are coloured in red, in the tetrahedral site in purple and oxygen atoms are displayed in blue.

Experimental setup. The X-ray diffraction data for PDF analysis application was collected at BL04-MSPD beamline in ALBA Synchrotron (Barcelona, Spain) using transmission Debye-Scherrer geometry with 0.5 mm borosilicate capillaries and a Mythen II linear position-sensitive detector. The photon energy used was 30 keV ($\lambda = 0.425127$ Å, refined using Si NIST SRM 640d). The measurements were performed over an angular domain (2θ) between 1.026 ° and 124.992 °, which provided a $Q_{\max}$ of 22 Å^{-1}. For resonant X-ray scattering analysis the data was collected at D10B-XPD beamline in LNLS (Campinas, Brazil) using reflection Bragg-Brentano geometry and a Cyberstar X1000 point detector. For this case energies close to the three absorption edges of Mn(6.528 keV), Fe (7.092 keV) and Zn (9.652 keV) were used. The measurements were performed over an angular domain (2θ) between 15.0 ° and 100.0 °, 30.0 ° and 91.8 ° and 11.0 ° and 78.5 ° for the energies close to the absorption edges of Mn, Fe and Zn, respectively.

Crystal structure description. – The spinel structure belongs to the $fd\bar{3}m$ space group (No. 227). Its cubic unit cell is formed by four tetragonal primitive unit cells. These primitive cells are composed by two units and can be represented by the AB_2O_4 formula, so each unit occupies one octant of the cubic unit cell. Between each oxygen there are 96 interstices, 64 of them are tetrahedral interstices and the remaining 32 are octahedral. Eight cations occupy the tetrahedral interstices and 16 cations occupy the octahedral interstices [8]. Conventionally, the tetrahedral cation sites are called A-sites whereas the octahedral sites are called B-sites. For ferrites that can be represented by $MeFe_2O_4$, A-sites are occupied by Me^{2+}cations, where Me refers to metal and B-sites are occupied by Fe^{3+}. See fig. 1 and table 1 for the structural atom positions.

If A-sites are completely occupied by Me^{2+} and Fe^{3+} fully occupies the B-sites, the structure is called normal

Table 1: The distribution of Mn-Zn ferrite atoms in the space group $Fd\bar{3}m$ (No. 227). $Z = 8$. Every site is represented by its multiplicity (m) and its Wycko? position (W).

Atom	Species	mW	x	y	z
Mn	Mn^{2+}	8a	1/4	1/4	1/4
Zn	Zn^{2+}	8a	1/4	1/4	1/4
Fe	Fe^{3+}	16d	1/2	1/2	1/2
O	O^{2-}	32e	x_O	x_O	x_O

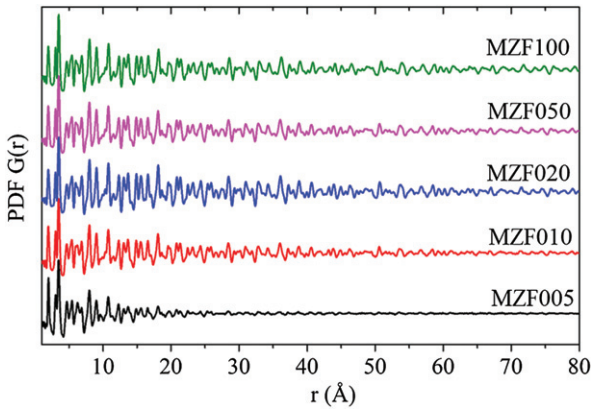

Fig. 2: (Colour online) Pair distribution function for the five samples of Mn-Zn ferrites precipitated with different NaOH concentrations.

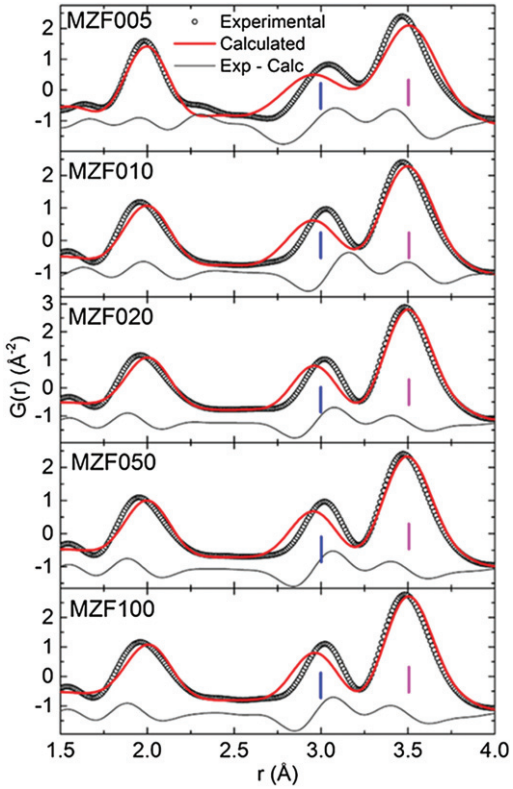

Fig. 3: (Colour online) PDF modelling for the five samples up to 4 Å, where the first-neighbour distances (Fe-Fe indicated by blue vertical lines and Mn-Zn by pink vertical lines) are not well modelled.

spinel, if the opposite occurs the structure is called inverse spinel. For Mn-Zn ferrites, the cations can occupy both sites, so the structure is referred to as mixed spinel [9]. Since, magnetic properties of such ferrites are strongly influenced by the cation distribution, its study is of paramount importance.

Results and discussion. – As can be seen from fig. 2, although MZF005 presents less structural coherence, it holds in the local structure features from the spinel configuration up to 20 Å. The MZF010 sample exhibits less short-range ordering than the other ones, terminating at approximately 50 Å. The other ones, apart from its nanocrystallinity, present visible PDF peaks up to 80 Å. The PDFs can be seen in fig. 2.

PDF modelling was performed to mainly study the first metal-metal sphere. As a starting point, values from the ICSD CIF file No. 170913 were used for the modelling. As can be seen in fig. 3, the model misses two peaks at approximately 3.0 and 3.5 Å, which correspond to the first-neighbour distances of Fe-Fe and Mn-Zn atoms, respectively.

The first PDF peak exhibits a shift towards right, whereas the second one shifts towards left, revealing that the Fe-Fe distance is larger and the Mn-Zn distance is shorter than expected. As pointed out by Antic *et al.* [10] this can be explained by the cation distribution in the spinel structure. Since Mn, Zn and Fe have different ionic radii its distribution within tetrahedral and octahedral sites can alter the pair distances causing the fluctuations observed in the PDF modelling. In fig. 4 the PDF modelling from 4 up to 20 Å presents a good fitting to the experimental data, which indicates that the average structure can be well described by the starting model.

To better access the cation distribution, RXS analysis was performed by means of Rietveld refinement for the sample with the best magnetic behaviour with energies close to the three absorption edges of Mn (6.528 keV), Fe (7.092 keV) and Zn (9.652 keV).The difference between the measurements can be seen in fig. 5, where the normalized integrated intensities of each reflection of the XRD profiles are presented. The main differences can be seen for the (4 0 0), (5 3 3) and (6 2 2) reflections.The best magnetic behaviour was found for MZF020, which was already confirmed in a previous study [11] that dealt with size-strain analysis of the crystallites and magnetic properties (accessed by magnetic saturation) of MZF010, MZF020, MZF050 and MZF100 samples. The refinements can be seen in fig. 6.

For RXS analysis, the energies were determined by refining the wavelength using Al_2O_3 NIST 676a SRM. The refinement strategy was to change and test many cation distribution possibilities, always simultaneously refining the profile for the three different energies. The best result was achieved when the cation distribution proposed by Mathew and Juang [9] was used. Mn, Zn and Fe occupy the A-site (tetrahedral) and Mn and Fe the B-site

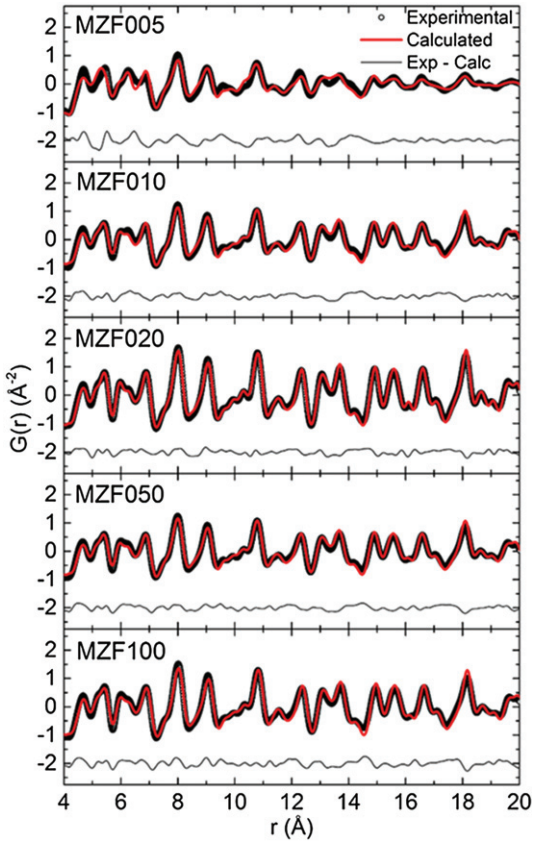

Fig. 4: (Colour online) PDF modelling for the five samples over 4 up to 20 Å, which gives a good agreement.

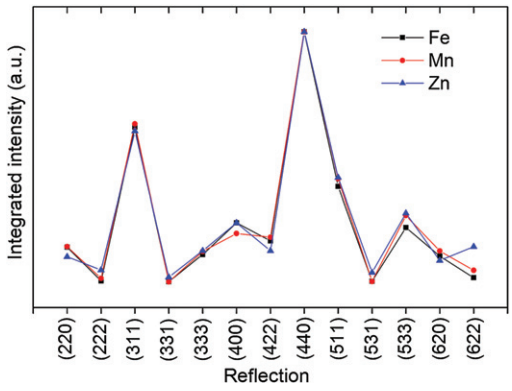

Fig. 5: (Colour online) Normalized integrated intensities for various XRD reflections measured near the absorption edges of Mn (6.528 keV), Fe (7.092 keV) and Zn (9.652 keV).

(octahedral). A refinement with a $R_{\rm wp} \sim 3.3\%$ was achieved. With this configuration it was possible to refine the ADP factors (overall) and occupancy with a very good estimation. Results are presented in table 2.

δ represents the so-called degree of inversion (defined as the fraction of A-site occupied by Fe^{3+} cations). In the above formula when $\delta < 0$ it is called normal spinel. When $\delta < 1$ it is called inverse spinel. When $0 < \delta < 1$ it is called mixed spinel. Also, with the refined occupancies it is possible to calculate the formal composition as $Mn_{0.7}Zn_{0.3}Fe_2O_4$.

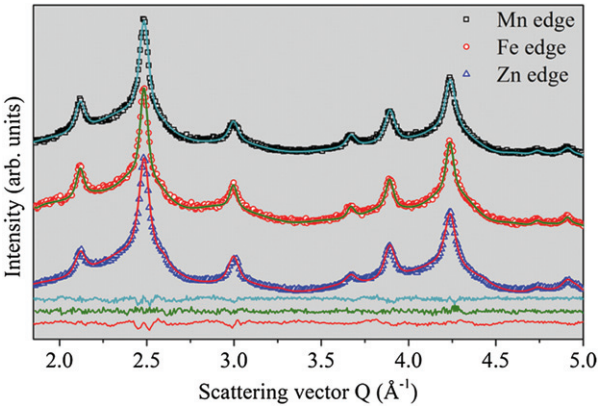

Fig. 6: (Colour online) Resonant X-ray scattering (RXS) data refinement for the MZF020 sample for the three energies close to the absorption edges of Mn, Fe and Zn.

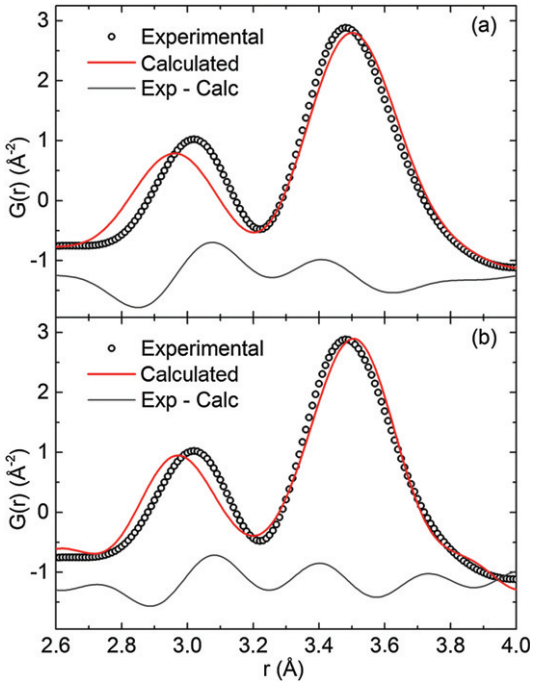

Fig. 7: (Colour online) PDF modelling for the MZF020 sample in the 2.6 up to 4 Å region.

Table 2: The distribution of Mn-Zn ferrite atoms in the space Group $fd\bar{3}m$ (No. 227). $Z = 8$. Every site is represented by its multiplicity (m) and its Wycko? position (W).

Parameter	Value
δ	0.60 (5)
a (nm)	0.83904 (13)
x_0	0.25157 (86)
$U_{\rm iso}$ (Å^2)	0.00024 (17)
D (nm)	9.5 (4)
$R_{\rm wp}$ (%)	3.3

Since Mn^{2+} has the larger ionic radius (0.96 Å) and is now sharing the octahedra site with Fe (for a octahedra coordination Fe have a ionic radius of 0.78 Å), this gives rise to smaller Mn-Zn distances, concomitantly Fe that now also occupies the tetrahedral site has a smaller ionic radius for a tetrahedral coordination (0.49 Å) which implies larger Fe-Fe pair distances.To verify this new cation distribution, the PDF refinement was performed again in the region below 4 Å for the MZF020 sample.

As can be seen from fig. 7, the modelling presented an improvement, especially for the 3.0 Å peak, which corresponds to the Fe-Fe distance. The minor differences can be attributed to the valence variation which was kept fixed as the ones in the CIF file. This variation can alter the radii of the considered atoms, contributing to the variation of the atom-atom distances. Also, the existence of a less crystalline phase as found in a previous work [11], can also contribute to the minor modelling mismatches in fig. 7. For the future, X-ray photoelectron spectroscopy experiments can be used to determine with precision the valence of the atoms.

Conclusion. – The local structure of Mn-Zn ferrite nanoparticles was analysed by PDF that showed a small distortion in the pair distances of Fe-Fe and Mn-Zn. This distortion can be related to the cation distribution in the spinel structure, confirmed by RXS for the sample precipitated with 0.20 mol/L. It was seen that the A-site is shared by Mn, Zn and Fe cations, whereas the B-site only by Mn and Fe. This comprises a mixed spinel structure with a degree of inversion of 0.60 (5). Besides that, it was possible to calculate its formal composition as $Mn_{0.7}Zn_{0.3}Fe_2O_4$. Finally, the two techniques, PDF and RXS, when applied concomitantly, have proven to be very useful to describe completely the local structure, in particular, the cation distribution.

* * *

RUI would like to acknowledge ALBA Synchrotron and MSPD beamline staff for the XRD measurements and LNLS (Proposal 20160591) for the resonant X-ray scattering measurements. IP is supported by the National Research Fund of Luxembourg (Grant No FNR-Inter2015/LRSF). XT would like to acknowledge the financial support from the Spanish MINECO projects MAT2015-67593-P and BIA2014-57658-C2-1-R. (MINECO) projects MAT2015-67593-P and BIA2014-57658-C2-1-R.

REFERENCES

[1] Martins M. L., Calabresi M. F., Quini C., Matos J. F., Miranda J. R., Saeki M. J. and Bordallo H. N., *Mater. Sci. Eng. C*, **48** (2015) 80.

[2] Parra J. P. R. L. L., Martins M. L., Moretto G. M., Ichikawa R. U., Martinez L. G., Corauto F., Miranda J. R. A. and Saeki M. J. F., in *Congress of Applied Physics to Medicine-CONFIAM, Botucatu, Brazil, 2014 (State University of São Paulo, Botucatu-SP)* 2014, pp. 1–2.

[3] Martins M. L., Saeki M. J., Telling M. T. F., Parra J. P. R. L. L., Landsgesell S., Smith R. I. A. and Bordallo H. N., *J. Alloys Compd.*, **584** (2014) 514.

[4] Billinge S. J. L., *Z. Kristallogr.*, **219** (2004) 117.

[5] Billinge S. J. L., in *Powder Diffraction: Theory and Practice*, edited by Dinnebier R. E. and Billinge S. J. L. (Cambridge University Press, Cambridge, UK) 2008, Chapt. 14, p. 464.

[6] Waseda Y., Shinoda K. and Sugiyama K., *Z. Naturforsch.*, **50a** (1995) 1199.

[7] Kohara S., Tajiri H., Song C. H., Ohara K., Temleitner L., Sugimoto K., Fujiwara A., Pusztai L., Usuki T., Hosokawa S., Benino Y., Kitamura N. and Fukumi K., *J. Phys.: Conf. Ser.*, **502** (2014) 012014.

[8] Sickafus K. E. and Wills J. M., *J. Am. Ceram. Soc.*, **82** (1999) 3279.

[9] Mathew D. S. and Juang R.-S., *Chem. Eng. J.*, **129** (2007) 51.

[10] Antic B., Perovic M., Kremenovic A., Blanusa J., Spasojevic V., Vulic P., Bessais L. and Bozin E. S., *J. Phys.: Condens. Matter.*, **25** (2013) 086001.

[11] Ichikawa R. U., Parra J. P. R. L. L., Martins M. L., Yoshito W. K., Saeki M. J., Turrillas X. and Martinez L. G., *J. Nanosci. Nanotechnol.*, **18** (2018) 5697.